,

SCIENCE CHINA
Information Sciences

• Supplementary File •

Hypersonic flight discrete-time optimal control with prescribed performance and saturation constraints

Xiangwei Bu[1*], Ruining Luo[1], Pengfei Wang[2] & Guangbin Cai[3]

[1]*Air Defense and Antimissile School, Air Force Engineering University, Xi'an 710051, China*
[2]*Army Arms University of PLA, Hefei 230031, China*
[3]*College of Missile Engineering, Rocket Force University of Engineering, Xi'an 710025, China*

Appendix A Motivation and contribution

Appendix A.1 Background

Contrast to optimal control strategies designed for continuous-time systems, discrete-time optimal control has received considerable attention owing to the pervasive use of digital systems in modern control applications [1]-[5], particularly in hypersonic flight systems (HFS), which constitute a class of long-range strategic transport aircraft. Discrete-time optimal control aims to stabilize dynamic systems while minimizing cost functions using dynamic programming methods, typically by solving the discrete-time Hamilton-Jacobi-Bellman (DHJB) equation. The policy iteration algorithm [6] is commonly employed to solve the DHJB equation, as demonstrated in seminal works [7], [8]. However, this algorithm requires an initial admissible control policy, which can be challenging to obtain in practical scenarios. To address this limitation, an alternative algorithm known as value iteration was introduced, and its convergence properties were rigorously proven for the first time by Al-Tamimi et al. [9]. Since then, value iteration has emerged as a novel approach offering local convergence benefits while significantly reducing computational burden and complexity [10].

The aforementioned dynamic programming-based optimal control methods inevitably face the challenge of the curse of dimensionality, a limitation that can be effectively mitigated through adaptive dynamic programming (ADP) strategies, also referred to as adaptive critic design (ACD) [11]-[13]. Over the past few decades, a wide range of ADP/ACD-based optimal control approaches has been developed for discrete-time systems. For example, Wei et al. [14] proposed a novel iterative algorithm for solving zero-sum differential games in discrete-time nonlinear dynamic systems, with theoretical convergence analysis and numerical simulations confirming its effectiveness and optimality. Liu et al. [15] investigated optimal tracking control for nonaffine systems with dead-zone inputs by employing neural networks to approximate optimal control policies within the ACD framework. Tang et al. [16] introduced an auxiliary compensation mechanism integrated with ACD for discrete-time systems affected by backlash-like hysteresis, achieving near-optimal control performance while compensating for non-affine couplings and hysteresis nonlinearities. Wang et al. [17] designed a state observer for state reconstruction and utilized estimation errors to simultaneously train both critic and actor networks based on high-order neural networks under the ACD architecture. Luo et al. [18] explored a data-driven optimal control strategy for constrained discrete-time systems, requiring only a critic network and ensuring that the resulting controller satisfies input saturation constraints. Dong et al. [19] sought to reduce computational overhead in time-updated neural network-based ADP by formulating enhanced adaptive laws that update neural network weights intermittently according to event-triggered mechanisms. Furthermore, significant attention has been devoted to optimal control of constrained dynamic systems. Bian et al. [1] developed a finite-time neuro-optimal control strategy for nonlinear systems subject to asymmetric constraints, integrating a Sub-Actor-Critic structure, identifier neural networks, and a policy iteration algorithm to ensure bounded system behavior and finite-time stability. Zhang et al. [2] proposed an anti-windup control framework for multimotor systems to handle dual saturation constraints, introducing a saturated super-twisting sliding mode control strategy that minimizes energy consumption while maintaining consistent traction performance across all motors. Wang et al. [3] formulated an optimal control problem for trajectory planning and derived the necessary conditions for optimality along with an associated optimal guidance law, further proposing a parameterized system to facilitate efficient generation of optimal trajectories and address challenges related to real-time implementation and convergence. Similarly, Chen et al. [4] addressed optimal trajectory planning by deriving necessary optimality conditions and an optimal guidance law, presenting a parameterized system to efficiently generate trajectories while focusing on practical issues concerning real-time execution and convergence properties.

Although ADP/ACD-based discrete-time optimal control methods have achieved considerable success, they do not guarantee predefined transient and steady-state performance of system outputs. Prescribed performance control (PPC), first introduced by Bechlioulis et al. [20], has proven to be an effective framework for enforcing desired dynamic behaviors in system responses. However, the majority of existing PPC research has focused on continuous-time systems [21], [22], with limited attention given to discrete-time counterparts. Current advances in discrete-time PPC include the followings. Yoshimura [23] proposed an approximate PPC scheme for uncertain discrete-time nonlinear systems in strict-feedback form, aiming to simplify control architecture and ensure stability under full-state constraints via adaptive fuzzy backstepping control. In another study, Yoshimura [24] developed a novel PPC approach for uncertain MIMO stochastic discrete-time nonlinear systems, emphasizing stability analysis and constrained control design using adaptive fuzzy backstepping techniques. In addition, Huang [25] presented a model-free adaptive sliding mode control method based on a discrete-time extended state observer, achieving prescribed tracking performance and effective estimation of disturbances and uncertainties.

Appendix A.2 Motivation

Despite that the aforementioned research progress is impressive, it reveals evident limitations that warrant further investigation and extension.

1. Currently, research on continuous-time PPC has achieved substantial progress, whereas studies on discrete-time PPC remain in the early developmental stage. However, directly discretizing existing continuous-time PPC methods and applying them to discrete-time systems may result in control failure, as such discretization can lead to instability of the closed-loop system. This is due to the availability of numerous well-established design strategies in the continuous-time domain that effectively guarantee system stability and achieve desired transient and steady-state performance. In contrast, these strategies do not translate effectively to the discrete-time domain. Therefore, given that most modern control systems are implemented digitally and operate in discrete time, the development of dedicated discrete-time PPC methodologies is both necessary and imperative.

2. Recently, several scholars have conducted preliminary investigations into discrete-time PPC [22]-[25]. However, it is important to note that all of these studies rely on a fixed design framework based on the sliding mode reaching law. This inherent limitation restricts the generalizability of their approaches to other discrete-time control methodologies and significantly undermines their practical applicability in real-world engineering contexts.

3. Despite significant advancements in optimal PPC for continuous-time dynamic systems [26]-[29], the extension to discrete-time optimal control problems with prescribed performance has been largely neglected. This gap poses a critical challenge: how can discrete-time optimal control strategies be developed to achieve desired prescribed performance? Given that most computer-based control systems operate in discrete time, there is an urgent need to establish discrete-time optimal control frameworks that guarantee both predefined performance and optimalityparticularly for hypersonic flight systems, which require exceptional transient response, steady-state accuracy, and overall control efficiency.

Appendix A.3 Contributions

Inspired by the above discussion, the primary objective of this letter is to develop an ADP-based optimal control framework for discrete-time dynamic systems with unknown nonlinearities, aiming to achieve predetermined system output behaviors. The key contributions of this study are as follows:

1. To the best of our knowledge, there is currently no discrete-time optimal control approach that simultaneously guarantees prescribed performance and accounts for actuator saturation constraints. This study aims to bridge this gap by introducing an asymptotic update mechanism to extend the discrete-time plant into an augmented dynamic system incorporating fixed-time prescribed performance characteristics. This formulation enables the development of an optimal control synthesis framework capable of achieving desired transient and steady-state performance in discrete time.

2. Existing discrete-time PPC methods [30]-[35] are predominantly confined within the sliding mode design (SMD) framework, which restricts their compatibility with other control methodologies and limits opportunities for performance enhancement. In contrast, the proposed discrete-time optimal PPC approach overcomes the structural limitations inherent in SMD, thereby broadening its theoretical applicability and potential for integration with advanced control strategies.

3. A novel cost function is formulated to derive discrete-time optimal PPC protocols, specifically tailored for application to hypersonic flight systems. The proposed design explicitly incorporates saturation constraints, addressing a critical limitation observed in existing adaptive dynamic programming (ADP) approaches [1]-[3], where control signals may exceed actuator limits during computation, leading to implementation failures in practical scenarios.

The overall structure unfolds as follows. A comprehensive exposition of the motivation and contributions graces Appendix A. The core findings, meticulously derived, are unveiled in Appendix B. The proposed strategy is brought to life through simulation-based validation in the context of hypersonic flight systems in Appendix C, and finally, the concluding insights are elegantly synthesized in Appendix D.

Appendix B Main results

Appendix B.1 System plant

Without loss of generality, we first consider a class of discrete-time systems with control actuators subject to saturation constraints. For these systems, a novel prescribed-time performance optimal control approach will be subsequently proposed and applied to hypersonic flight systems.

$$x_{k+1} = f(x_k) + g(x_k)u_k, \tag{B1}$$

where $x_k = [x_{1,k}, x_{2,k}, \cdots, x_{n,k}]^\top \in \Re^n$ is the system state, $u_k = [u_{1,k}, u_{2,k}, \cdots, u_{m,k}]^\top \in \Re^m$ is the control input with saturation constraint $-\bar{u} \leqslant u_k \leqslant \bar{u} = [\bar{u}_1, \bar{u}_2, \cdots, \bar{u}_m]^\top \in \Re^m_{>0}$, $\bar{u}$ is the upper bound of u_k, $f(x_k) : \Re^n \mapsto \Re^n$ and

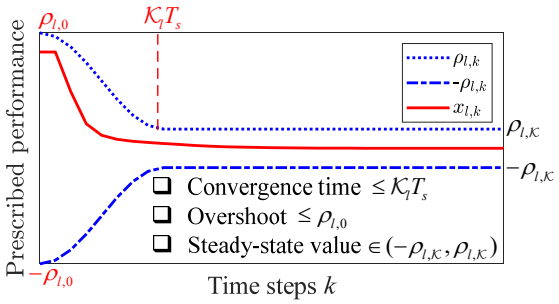

Figure B1 Boundary constraint on x_k.

$g(x_k) : \Re^n \mapsto \Re^{n\times m}$ are continuous functions of x_k satisfying $f(x_k)|_{x_k=0} = 0$, so that $x_k = 0$ is the equilibrium state of (B1) under $u_k = 0$, the positive integers $m \in \mathcal{Z}_{>0}$ and $n \in \mathcal{Z}_{>0}$ denote the number of control input and system state, respectively, and $k = 0 : 1 : \infty$ is the time index/step.

The control synthesis for (B1) requires the priori knowledge [9] that the system (B1) can be stabilizable on a compact set $\Omega_x \subseteq \Re^n$ (At least one admissible control u_k exists that for all $x_k|_{k=0} \in \Omega_x \subseteq \Re^n$, the state $x_k|_{k\to\infty} \to 0$). Though existing studies [1]-[3] are capable of optimally stabilizing the system (B1), all of them fail to meanwhile achieve prescribed transient and steady-state qualities for x_k. In the following subsection, pioneering work will be presented to guarantee x_k with those predetermined transient and steady-state behaviors, by limiting x_k within a prescribed boundary in the discrete-time domain.

Appendix B.2 Fixed-time prescribed performance

For the sake of guaranteeing the system state x_k of (B1) with a novel type of fixed-time prescribed performance (B3), we firstly devise the following discrete-time performance function $\rho_{l,k} \in \Re_{>0}$

$$\rho_{l,k} = \begin{cases} \rho_l^- \tanh\left(\pi - \frac{2\pi}{\mathcal{K}_l} k\right) + \rho_l^+, k \leqslant \mathcal{K}_l \\ \rho_{l,\mathcal{K}}, k > \mathcal{K}_l, \end{cases} \tag{B2}$$

where $l = 1 : 1 : n$, the positive integer $\mathcal{K}_l \in \mathcal{Z}_{>0}$ means the required steps for $\rho_{l,k}$ to convergence from its initial value $\rho_{l,0} = \rho_{l,k}\big|_{k=0} \in \Re_{>0}$ to its state-sate value $\rho_{l,\mathcal{K}} = \rho_{l,k}\big|_{k>\mathcal{K}_l} \in \Re_{>0}$, so that $\rho_{l,0}$ should be larger than $\rho_{l,\mathcal{K}}$, and ρ_l^- and ρ_l^+ are defined as $\rho_l^- = \frac{\rho_{l,0}}{2} - \frac{\rho_{l,\mathcal{K}}}{2}$ and $\rho_l^+ = \frac{\rho_{l,0}}{2} + \frac{\rho_{l,\mathcal{K}}}{2}$.

By fixed-time prescribed performance, we mean that x_k should always evolve within the boundary

$$-\rho_{l,k} < x_{l,k} < \rho_{l,k}, l = 1 : 1 : n. \tag{B3}$$

Remak 1. The boundary constraint on x_k and the physical meanings of design parameters are illustrated in Fig. B1. The boundary constraint on x_k is illustrated in Fig. B1. With such envelope constraint, all the states of (B1) satisfy the fixed-time prescribed performance: 1) the convergence time isnt than $\mathcal{K}_l T_s$ where $T_s \in \Re_{>0}$ is the sampling period, 2) the overshoot is less than $\rho_{l,0}$, and 3) the steady-state value is within $(-\rho_{l,\mathcal{K}}, \rho_{l,\mathcal{K}})$ with $l = 1 : 1 : n$, so that all states of (B1) are able to converge to the steady-state values within a fixed-time, and meanwhile both transient and steady-state qualities can be achieved by devising suitable parameters for $\rho_{l,k}$. The physical meanings of the above parameters provide valuable guidance for parameter selection in practical applications. For instance, in flight control systems, appropriate values for the design parameters can be determined based on specific performance requirementssuch as overshoot, steady-state error, and convergence timeand the established relationships between these parameters and the corresponding performance metrics, thereby enabling the achievement of desired control performance objectives.

To limit x_k within the boundary (B3), by the PPC theory [20], we should further define the transformed error $\alpha_{l,k} \in \Re$

$$\alpha_{l,k} = \frac{1}{2} \ln\left(\frac{\rho_{l,k} + x_{l,k}}{\rho_{l,k} - x_{l,k}}\right), l = 1 : 1 : n. \tag{B4}$$

The prescribed performance (B3) for continuous-time PPC [21]-[23] can be easily ensured by stabilizing the dynamic system to ensure boundedness of $\alpha_{l,k} \in \Re$. However, in the discrete-time domain, the existing SMC-based framework [30] fails to construct an effective PPC methodology that achieves control optimality. To address this limitation, we propose an Inverse Thinking approach, whereby a novel asymptotic iteration for $\alpha_{l,k} \in \Re$ is first developed, and subsequently used to derive a new dynamic system that facilitates the design of discrete-time optimal PPC. The asymptotic iteration for $\alpha_{l,k} \in \Re$ is defined as follows.

$$\alpha_{l,k+1} = \frac{1}{2} \ln\left(\frac{\rho_{l,k+1} + x_{l,k+1}}{\rho_{l,k+1} - x_{l,k+1}}\right) := \eta_l \alpha_{l,k}, \tag{B5}$$

with $-1 < \eta_l < 1$ and $l = 1 : 1 : n$.

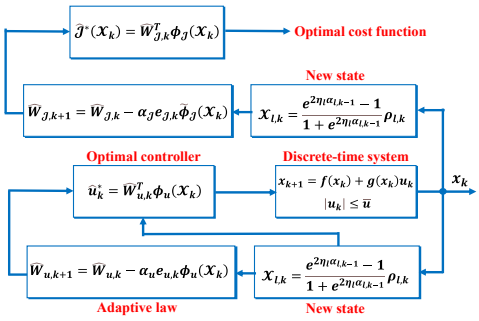

Figure B2 Diagram of the control system.

It is observed from (B5) that

$$x_{l,k+1} = \frac{e^{2\eta_l \alpha_{l,k}} - 1}{1 + e^{2\eta_l \alpha_{l,k}}} \rho_{l,k+1} := \mathcal{X}_{l,k+1}, l = 1:1:n. \tag{B6}$$

In view of (B1) and (B6), we easily construct a new dynamic system

$$\mathcal{X}_{k+1} = f(\mathcal{X}_k) + g(\mathcal{X}_k) u_k, \tag{B7}$$

with $\mathcal{X}_k = [\mathcal{X}_{1,k}, \mathcal{X}_{2,k}, \cdots, \mathcal{X}_{n,k}]^\top \in \Re^n$, $\mathcal{X}_{l,k} = \frac{e^{2\eta_l \alpha_{l,k-1}} - 1}{1 + e^{2\eta_l \alpha_{l,k-1}}} \rho_{l,k}$, and $l = 1:1:n$.

Remak 2. According to Definition (B5), it follows that $L_{l,k} = \alpha_{l,k}^2 \Rightarrow \nabla L_{l,k} = \alpha_{l,k+1}^2 - \alpha_{l,k}^2 = (\eta_l^2 - 1)\alpha_{l,k}^2 \leqslant 0$, which implies that the defined iteration (B5) is asymptotically convergent. Furthermore, it is observed that systems (B7) and (B1) share identical formulations. Therefore, the new system (B7) is also stabilizable, with $\mathcal{X}_k = 0$ being its equilibrium state. In the following analysis, system (B7)rather than system (B1)will be employed to design constrained optimal control protocols, which are intended for implementation in system (B1), such that the desired prescribed-time performance (B3) can be achieved. This leads naturally to a novel framework that differs from the existing SMC-driven PPC structures [30]-[35], providing an effective approach for prescribed performance optimal control synthesis.

Appendix B.3 Control aim

In this article, the control synthesis aims to find a saturated optimal controller u_k^*, which is constrained by $u_k^* \in [-\bar{u}, \bar{u}]$, to maintain the system state x_k, starting from any initial point $x_k|_{k=0} \in \Omega_x \subseteq \Re^n$, at its equilibrium state $x_k = 0$, with the convergence trajectory of x_k satisfying desired prescribed performance (B3), and also to minimize the following cost function

$$\mathcal{J}(\mathcal{X}_k) = \sum_{j=k}^{\infty} (\mathcal{X}_j^\top \mathcal{Q}_\mathcal{X} \mathcal{X}_j + \mathcal{W}(u_j)) = r(\mathcal{X}_k, u_k) + \mathcal{J}(\mathcal{X}_{k+1}), \tag{B8}$$

with $r(\mathcal{X}_k, u_k) = \mathcal{X}_k^\top \mathcal{Q}_\mathcal{X} \mathcal{X}_k + \mathcal{W}(u_k)$, $\mathcal{W}(u_j) = 2\int_0^{u_j} \text{atanh}^\top\left(\frac{\tau}{\bar{u}}\right) \mathcal{R}_u \bar{u} d\tau$, and $\text{atanh}\left(\frac{\tau}{\bar{u}}\right) = \left[\text{atanh}\left(\frac{\tau}{\bar{u}_1}\right), \cdots, \text{atanh}\left(\frac{\tau}{\bar{u}_m}\right)\right]^T$, where τ is the integration variable, and $\mathcal{Q}_\mathcal{X} \in \Re^{n\times n}$ and $\mathcal{R}_u \in \Re^{m\times m}$ are positive definite symmetric matrices. In (B8), the infinite-horizon cost function (B8) is necessary for the considered control problem, as the finite-horizon cost function is typically applicable to dynamic programming problemsensuring state evolution from current to final values. In contrast, for control design problems, an infinite-horizon performance function must be adopted, which not only ensures the transition of states from their current values to the desired final values but also guarantees that the states remain at these final values (i.e., the equilibrium points) indefinitely.

Appendix B.4 Prescribed performance optimal control design

By Bellman's optimality principle, we can derive the optimal cost function $\mathcal{J}^*(\mathcal{X}_k)$ via solving the following discrete-time HJB equation

$$\mathcal{J}^*(\mathcal{X}_k) = \min_{-\bar{u} \leqslant u_k \leqslant \bar{u}} \{r(\mathcal{X}_k, u_k) + \mathcal{J}^*(\mathcal{X}_{k+1})\}. \tag{B9}$$

From (B9), we further get the optimal controller u_k^*, as shown in Fig. B2

$$u_k^* = \arg \min_{-\bar{u} \leqslant u_k \leqslant \bar{u}} \{r(\mathcal{X}_k, u_k) + \mathcal{J}^*(\mathcal{X}_{k+1})\}. \tag{B10}$$

The existence of saturation constraint (i.e., $-\bar{u} \leqslant u_k \leqslant \bar{u}$) leads to the failure of existing solution methods for u_k^* [1]-[3]. Thanks to the newly defined cost function (B8), we can still solve for u_k^*, which satisfies the saturation constraint $-\bar{u} \leqslant u_k^* \leqslant \bar{u}$, by taking partial derivatives of the right side of (B10) with respective to u_k.

$$0 = \frac{\partial r(\mathcal{X}_k, u_k)}{\partial u_k} + \frac{\partial \mathcal{X}_{k+1}^\top}{\partial u_k} \frac{\partial \mathcal{J}^*(\mathcal{X}_{k+1})}{\partial \mathcal{X}_{k+1}} \Rightarrow u_k^* = \bar{u} \tanh\left(\frac{v_k^*}{\bar{u}}\right), \tag{B11}$$

Algorithm 1: value iteration algorithm

Initialization: Set $\bar{u}$, $\varepsilon_{\mathcal{J}} \in \Re_{>0}$, $\varepsilon_u \in \Re_{>0}$, and $N \in \mathcal{Z}_{>0}$. Define $\rho_{l,k}$, $\alpha_{l,k}$, $\mathcal{X}_k$, and $\mathcal{J}(\mathcal{X}_k)$.

Output: u_k^* and $\mathcal{J}^*(\mathcal{X}_k)$.

while $i \leqslant N$ **do**
  Iterate $u_{i,k}$ via (B12);
  Iterate $\mathcal{J}_{i+1}(\mathcal{X}_k)$ via (B13);
  if $|\mathcal{J}_{i+1}(\mathcal{X}_k) - \mathcal{J}_i(\mathcal{X}_k)| \leqslant \varepsilon_{\mathcal{J}}$ and $||u_{i+1,k} - u_{i,k}|| \leqslant \varepsilon_u$ or $i \geqslant N$;
  then $\mathcal{J}^*(\mathcal{X}_k) \leftarrow \mathcal{J}_i(\mathcal{X}_k)$ and $u_k^* \leftarrow u_{i,k}$;
  break
  else
    $i \leftarrow i + 1$;
  end if
end while

with $\upsilon_k^* = -\frac{1}{2\bar{u}}\mathcal{R}_u^{-1} g^\top(\mathcal{X}_k)\frac{\partial \mathcal{J}^*(\mathcal{X}_{k+1})}{\partial \mathcal{X}_{k+1}}$.

Remak 3. It can be seen from (B11) that $u_k^* = \bar{u}$ if $\upsilon_k^* \geqslant \bar{u}$, $u_k^* = -\bar{u}$ if $\upsilon_k^* \geqslant -\bar{u}$, and otherwise $-\bar{u} \leqslant u_k^* \leqslant \bar{u}$, so that the calculated optimal controller $u_k^* = \bar{u}\tanh\left(\frac{\upsilon_k^*}{\bar{u}}\right)$ is always within the saturated bound $[-\bar{u}, \bar{u}]$. This avoids a practical scenario [28] where there is a risk of control failure that the obtained control value exceeds its reasonable range, making it impossible to be actually executed.

Subsequently, both the optimal cost function and controller will be determined using the value iteration algorithm [9]. By setting a zero initial cost function $\mathcal{J}_0(\mathcal{X}_k) = 0$, we get the i-th iteration for the control protocol

$$\begin{aligned} u_{i,k} =& \arg \min_{-\bar{u} \leqslant u_k \leqslant \bar{u}} \{r(\mathcal{X}_k, u_k) + \mathcal{J}_i(\mathcal{X}_{k+1})\} \\ =& \arg \min_{-\bar{u} \leqslant u_k \leqslant \bar{u}} \{\mathcal{X}_k^\top \mathcal{Q}_{\mathcal{X}} \mathcal{X}_k + \mathcal{W}(u_k) + \mathcal{J}_i(\mathcal{X}_{k+1})\} \\ =& \bar{u}\tanh\left(-\frac{1}{2\bar{u}}\mathcal{R}_u^{-1} g^\top(\mathcal{X}_k)\frac{\partial \mathcal{J}_i(\mathcal{X}_{k+1})}{\partial \mathcal{X}_{k+1}}\right), \end{aligned} \tag{B12}$$

with $i = 0:1:\infty$.

The $(i+1)$-th iteration for the cost function is given by

$$\begin{aligned} \mathcal{J}_{i+1}(\mathcal{X}_k) =& \min_{-\bar{u} \leqslant u_k \leqslant \bar{u}} \{r(\mathcal{X}_k, u_k) + \mathcal{J}_i(\mathcal{X}_{k+1})\} \\ =& \min_{-\bar{u} \leqslant u_k \leqslant \bar{u}} \{\mathcal{X}_k^\top \mathcal{Q}_{\mathcal{X}} \mathcal{X}_k + \mathcal{W}(u_k) + \mathcal{J}_i(\mathcal{X}_{k+1})\} \\ =& \mathcal{X}_k^\top \mathcal{Q}_{\mathcal{X}} \mathcal{X}_k + \mathcal{W}(u_{i,k}) + \mathcal{J}_i(f(\mathcal{X}_k) + g(\mathcal{X}_k)u_{i,k}), \end{aligned} \tag{B13}$$

with $i = 0:1:\infty$.

The above iterations can be summarized as Algorithm 1

Appendix B.5 Convergence proof

In this section, we will rigorously demonstrate the convergence of Algorithm 1 and establish the attainment of the defined prescribed performance (B3). To facilitate the subsequent proof, we first introduce the following lemmas.

Lemma 1 [9]. Define $\{\mu_{i,k} \in \Re^m\}$ as the arbitrary control sequence and update $\mathcal{J}_{i+1}(\mathcal{X}_k)$ via (B13). We then conclude $\mathcal{J}_{i+1}(\mathcal{X}_k) \leqslant V_{i+1}(\mathcal{X}_k)$ with $\mathcal{J}_0(\mathcal{X}_k) = V_0(\mathcal{X}_k) = 0$ and

$$V_{i+1}(\mathcal{X}_k) = \mathcal{X}_k^\top \mathcal{Q}_{\mathcal{X}} \mathcal{X}_k + \mathcal{W}(\mu_{i,k}) + V_i(f(\mathcal{X}_k) + g(\mathcal{X}_k)\mu_{i,k}). \tag{B14}$$

Lemma 2 [9]. For $i = 0:1:\infty$, the cost function $\mathcal{J}_i(\mathcal{X}_k)$, being solved from (B13), satisfies: 1) there exists an upper bound $\bar{\mathcal{J}}(\mathcal{X}_k) \in \Re_{>0}$ so that $0 \leqslant \mathcal{J}_i(\mathcal{X}_k) \leqslant \bar{\mathcal{J}}(\mathcal{X}_k)$; and 2) $0 \leqslant \mathcal{J}_i(\mathcal{X}_k) \leqslant \mathcal{J}^*(\mathcal{X}_k) \leqslant \bar{\mathcal{J}}(\mathcal{X}_k)$.

Lemma 3 [36]. For $l = 1:1:n$, the boundedness of the transformed error $\alpha_{l,k}$ can be guaranteed if the system (B7) is stabilized so that its state $\mathcal{X}_{l,k}$ is bounded. This also indicates that the defined prescribed performance (B3) can be achieved under such conditions.

To enhance the convergence proof, we present the following theorem.

Theorem 1. Considering the closed-loop system consisting of system (B1), control sequence (B12), and cost function sequence (B13) with $\mathcal{J}_0(\mathcal{X}_k) = 0$, we obtain:

1. For $i = 0:1:\infty$, we get $\mathcal{J}_i(\mathcal{X}_k) \leqslant \mathcal{J}_{i+1}(\mathcal{X}_k)$ with $\mathcal{J}_0(\mathcal{X}_k) = V_0(\mathcal{X}_k) = 0$;
2. As $i \to \infty$, we get $u_{i,k} \to u_k^*$ and $\mathcal{J}_i(\mathcal{X}_k) \to \mathcal{J}^*(\mathcal{X}_k)$, i.e., $u_{\infty,k} = u_k^*$ and $\mathcal{J}_\infty(\mathcal{X}_k) = \mathcal{J}^*(\mathcal{X}_k)$;

3. The expected prescribed performance (B3) is achievable.

Proof. We will prove Theorem 1 step-by-step.

- *Proof of the first item.*

Let $\mu_{i,k} = u_{i+1,k}$. In view of Lemma 1, we have

$$\begin{aligned} V_{i+1}(\mathcal{X}_k) =& \mathcal{X}_k^\top \mathcal{Q}_\mathcal{X} \mathcal{X}_k + \mathcal{W}(u_{i+1,k}) + V_i(f(\mathcal{X}_k) + g(\mathcal{X}_k)u_{i+1,k}) \\ \Downarrow& \\ V_i(\mathcal{X}_k) =& \mathcal{X}_k^\top \mathcal{Q}_\mathcal{X} \mathcal{X}_k + \mathcal{W}(u_{i,k,k}) + V_{i-1}(f(\mathcal{X}_k) + g(\mathcal{X}_k)u_{i,k}), \end{aligned} \tag{B15}$$

with $i = 0:1:\infty$.

The first item will be proved utilizing the inductive method.

1. Firstly, we note that $\mathcal{J}_0(\mathcal{X}_k) = V_0(\mathcal{X}_k) = 0$, so that $\mathcal{J}_0(\mathcal{X}_k) - V_1(\mathcal{X}_k) = -V_1(\mathcal{X}_k) \leqslant 0 \Rightarrow \mathcal{J}_0(\mathcal{X}_k) \leqslant V_1(\mathcal{X}_k)$.
2. By assuming that $\mathcal{J}_i(\mathcal{X}_k) \leqslant V_{i-1}(\mathcal{X}_k)$, we then prove $\mathcal{J}_{i+1}(\mathcal{X}_k) \leqslant V_{i+1}(\mathcal{X}_k)$, with $i = 0:1:\infty$.
3. Invoking (B13) and (B15)

$$\begin{aligned} V_i(\mathcal{X}_k) - \mathcal{J}_{i+1}(\mathcal{X}_k) =& V_{i-1}(f(\mathcal{X}_k) + g(\mathcal{X}_k)u_{i,k}) - \mathcal{J}_i(f(\mathcal{X}_k) + g(\mathcal{X}_k)u_{i,k}) \\ =& V_{i-1}(\mathcal{X}_{k+1}) - \mathcal{J}_i(\mathcal{X}_{k+1}) \leqslant 0 \Rightarrow V_i(\mathcal{X}_k) \leqslant \mathcal{J}_{i+1}(\mathcal{X}_k). \end{aligned} \tag{B16}$$

It has been proved by Lemma 1 that $\mathcal{J}_{i+1}(\mathcal{X}_k) \leqslant V_{i+1}(\mathcal{X}_k)$. We thereby get $V_i(\mathcal{X}_k) \leqslant \mathcal{J}_{i+1}(\mathcal{X}_k) \leqslant V_{i+1}(\mathcal{X}_k) \Rightarrow V_i(\mathcal{X}_k) \leqslant V_{i+1}(\mathcal{X}_k)$.

This completes the proof of the first item.

- *Proof of the second item.*

As $i \to \infty$, we conclude from (B13) that

$$\begin{aligned} \mathcal{J}_\infty(\mathcal{X}_k) =& \mathcal{X}_k^\top \mathcal{Q}_\mathcal{X} \mathcal{X}_k + \mathcal{W}(u_{\infty,k}) + \mathcal{J}_\infty(f(\mathcal{X}_k) + g(\mathcal{X}_k)u_{\infty,k}) \\ =& \mathcal{X}_k^\top \mathcal{Q}_\mathcal{X} \mathcal{X}_k + \mathcal{W}(u_{\infty,k}) + \mathcal{J}_\infty(\mathcal{X}_{k+1}) \\ \Downarrow& \\ \Delta\mathcal{J}_\infty(\mathcal{X}_k) =& \mathcal{J}_\infty(\mathcal{X}_{k+1}) - \mathcal{J}_\infty(\mathcal{X}_k) = -\mathcal{X}_k^\top \mathcal{Q}_\mathcal{X} \mathcal{X}_k - \mathcal{W}(u_{\infty,k}) \leqslant 0. \end{aligned} \tag{B17}$$

The positive-definite function $\mathcal{J}_\infty(\mathcal{X}_k)$ is a Lyapunov function candidate and its difference $\Delta\mathcal{J}_\infty(\mathcal{X}_k)$ is negative definite, so that we know $\mathcal{J}_\infty(\mathcal{X}_k) = \bar{\mathcal{J}}(\mathcal{X}_k)$. Lemma 2 shows that $\mathcal{J}^*(\mathcal{X}_k) \leqslant \mathcal{J}_\infty(\mathcal{X}_k)$. By the combination of Lemma 2 and the first item of Theorem 1, we further obtain $\mathcal{J}_i(\mathcal{X}_k) \to \mathcal{J}_\infty(\mathcal{X}_k) \leqslant \mathcal{J}^*(\mathcal{X}_k)$ as $i \to \infty$. We finally get $\mathcal{J}_\infty(\mathcal{X}_k) \leqslant \mathcal{J}^*(\mathcal{X}_k) \leqslant \mathcal{J}_\infty(\mathcal{X}_k) \Rightarrow \mathcal{J}_\infty(\mathcal{X}_k) = \mathcal{J}^*(\mathcal{X}_k)$, which also reveals that $u_{\infty,k} = u_k^*$ according the definition of $\mathcal{J}^*(\mathcal{X}_k)$. This completes the proof of the second item.

- *Proof of the third item.*

The second item of Theorem 1 has demonstrated that $u_{i,k} \to u_k^*$ as $i \to \infty$. Because u_k^* is an admissible control, the state $\mathcal{X}_k$ must be bounded and also satisfies that $\mathcal{X}_k \to 0$ as $k \to \infty$.

The desired prescribed performance (B3) is thus attained, as demonstrated by Lemma 3. This concludes the proof of the third item, thereby completing the proof of Theorem 1.

Remak 4. Theorem 1 proves the convergence of iteration algorithm 1, which also indicates that the defined prescribed performance (B3) can be guaranteed for x_k. To the best of our knowledge, there is currently no discrete-time optimal control scheme that can achieve such predetermined transient and steady-state behaviors. As proved in Theorem 1, we theoretically get that $u_{i,k} \to u_k^*$ and $\mathcal{J}_i(\mathcal{X}_k) \to \mathcal{J}^*(\mathcal{X}_k)$ only when $i \to \infty$. Hence, in practical applications, the ADP approach is typically employed to approximate the algorithm.

Appendix C Application to hypersonic flight systems via simulation validation

In this section, the proposed controller is approximately implemented using the ADP approach (see Fig. B2), with simulation validation conducted in MATLAB 2024b that is a platform widely adopted in the control systems domain to verify the precision and effectiveness of control strategies. The simulation comprises the following examples.

Appendix C.1 Example 1

The addressed controller is applied to a first-order system $x_{k+1} = f(x_k) + g(x_k)u_k$ with $f(x_k) = x_k \in \Re$, $g(x_k) = 1$, and $u_k \in \Re$. It is obvious that $x_k = 0$ is the equilibrium state. The state x_k satisfies the prescribed performance $-\rho_k < x_k < \rho_k$ with

$$\rho_k = \begin{cases} \rho^- \tanh\left(\pi - \frac{2\pi}{\mathcal{K}}k\right) + \rho^+, k \leqslant \mathcal{K} \\ \rho_\mathcal{K}, k > \mathcal{K}, \end{cases} \tag{C1}$$

where $\rho^- = \frac{\rho_0}{2} - \frac{\rho_\mathcal{K}}{2}$, $\rho^+ = \frac{\rho_0}{2} + \frac{\rho_\mathcal{K}}{2}$, and $\mathcal{K}$ is a positive integer.

Define the transformed error $\alpha_k = \frac{1}{2}\ln\left(\frac{\rho_k + x_k}{\rho_k - x_k}\right)$. From (B6), we get a new state $\mathcal{X}_{k+1} = \frac{e^{2\eta\alpha_k}-1}{1+e^{2\eta\alpha_k}}\rho_{k+1}$ and a new dynamic system $\mathcal{X}_{k+1} = f(\mathcal{X}_k) + g(\mathcal{X}_k)u_k$ with $\eta = 0.45$. Define the cost function $\mathcal{J}(\mathcal{X}_k) = \sum_{j=k}^{\infty}(\mathcal{X}_j^\top \mathcal{Q}_\mathcal{X}\mathcal{X}_j + \mathcal{W}(u_j))$ with $\mathcal{W}(u_j) = 2\int_0^{u_j} \text{atanh}^\top\left(\frac{\tau}{\bar{u}}\right)\mathcal{R}_u\bar{u}d\tau = \mathcal{R}_u\bar{u}^2\ln\left(1-\frac{u_j^2}{\bar{u}^2}\right) + 2\mathcal{R}_u\bar{u}u_j\text{atanh}\left(\frac{u_j}{\bar{u}}\right)$.

Inspired by [37], the optimal controller u_k^* and the optimal cost function $\mathcal{J}^*(\mathcal{X}_k)$ are approximately estimated as follows:

$$\hat{u}_k^* = \hat{W}_{u,k}^\top \phi_u(\mathcal{X}_k), \hat{\mathcal{J}}^*(\mathcal{X}_k) = \hat{W}_{\mathcal{J},k}^\top \phi_\mathcal{J}(\mathcal{X}_k), \tag{C2}$$

where $\hat{u}_k^*$ and $\hat{\mathcal{J}}^*(\mathcal{X}_k)$ are the estimations of u_k^* and $\mathcal{J}^*(\mathcal{X}_k)$, respectively, with

$$\begin{cases} \hat{W}_{u,k} = [\hat{\omega}_{u1,k}, \hat{\omega}_{u2,k}, \hat{\omega}_{u3,k}, \hat{\omega}_{u4,k}, \hat{\omega}_{u5,k}]^\top \in \Re^5 \\ \hat{W}_{\mathcal{J},k} = [\hat{\omega}_{\mathcal{J}1,k}, \hat{\omega}_{\mathcal{J}2,k}, \hat{\omega}_{\mathcal{J}3,k}, \hat{\omega}_{\mathcal{J}4,k}, \hat{\omega}_{\mathcal{J}5,k}]^\top \in \Re^5 \\ \phi_u(\mathcal{X}_k) = \phi_\mathcal{J}(\mathcal{X}_k) = [\mathcal{X}_k, \mathcal{X}_k^2, \mathcal{X}_k^3, \mathcal{X}_k^4, \mathcal{X}_k^5]^\top \\ \hat{W}_{u,0} = [-0.8, -0.26, -0.14, -0.08, -0.08]^\top \\ \hat{W}_{\mathcal{J},0} = [0.09, 0.06, 0.04, 0.2, 0.2]^\top. \end{cases}$$

Define the controller estimation error $e_{u,k}$ and the cost function estimate error $e_{\mathcal{J},k}$ as

$$e_{u,k} = -\bar{u}\tanh\left(-\frac{1}{2\bar{u}}\mathcal{R}_u^{-1}g^\top(\mathcal{X}_k)\frac{\partial\hat{\mathcal{J}}^*(\mathcal{X}_{k+1})}{\partial\mathcal{X}_{k+1}}\right) + \hat{W}_{u,k}^T\phi_u(\mathcal{X}_k), \tag{C3}$$

$$e_{\mathcal{J},k} = \mathcal{X}_k^\top\mathcal{Q}_\mathcal{X}\mathcal{X}_k + \mathcal{W}(u_k) + \hat{\mathcal{J}}^*(\mathcal{X}_{k+1}) - \hat{\mathcal{J}}^*(\mathcal{X}_k) = \mathcal{X}_k^T\mathcal{Q}_\mathcal{X}\mathcal{X}_k + \mathcal{W}(u_k) + \hat{W}_{\mathcal{J},k}^\top\tilde{\phi}_\mathcal{J}(\mathcal{X}_k), \tag{C4}$$

with

$$\frac{\partial\hat{\mathcal{J}}^*(\mathcal{X}_{k+1})}{\partial\mathcal{X}_{k+1}} = \hat{\omega}_{\mathcal{J}1,k} + 2\hat{\omega}_{\mathcal{J}2,k}\mathcal{X}_{k+1} + 3\hat{\omega}_{\mathcal{J}3,k}\mathcal{X}_{k+1}^2 + 4\hat{\omega}_{\mathcal{J}4,k}\mathcal{X}_{k+1}^3 + 5\hat{\omega}_{\mathcal{J}5,k}\mathcal{X}_{k+1}^4, \tag{C5}$$

$$\tilde{\phi}_\mathcal{J}(\mathcal{X}_k) = \phi_\mathcal{J}(\mathcal{X}_{k+1}) - \phi_\mathcal{J}(\mathcal{X}_k) = \begin{bmatrix} \mathcal{X}_{k+1} - \mathcal{X}_k \\ \mathcal{X}_{k+1}^2 - \mathcal{X}_k^2 \\ \mathcal{X}_{k+1}^3 - \mathcal{X}_k^3 \\ \mathcal{X}_{k+1}^4 - \mathcal{X}_k^4 \\ \mathcal{X}_{k+1}^5 - \mathcal{X}_k^5 \end{bmatrix}, \tag{C6}$$

$$\mathcal{X}_{k+1} = f(\mathcal{X}_k) + g(\mathcal{X}_k)\hat{W}_{u,k}^\top\phi_u(\mathcal{X}_k). \tag{C7}$$

Employing the gradient-based adaptation [10] to minimize $E_{u,k} = \frac{1}{2}e_{u,k}^2$ and $E_{\mathcal{J},k} = \frac{1}{2}e_{\mathcal{J},k}^2$, we develop the following adaptive laws for $\hat{W}_{u,k}$ and $\hat{W}_{\mathcal{J},k}$

$$\hat{W}_{u,k+1} = \hat{W}_{u,k} - \alpha_u\frac{\partial E_{u,k}}{\partial e_{u,k}}\frac{\partial e_{u,k}}{\partial\hat{W}_{u,k}} = \hat{W}_{u,k} - \alpha_u e_{u,k}\phi_u(\mathcal{X}_k), \tag{C8}$$

$$\hat{W}_{\mathcal{J},k+1} = \hat{W}_{\mathcal{J},k} - \alpha_\mathcal{J}\frac{\partial E_{\mathcal{J},k}}{\partial e_{\mathcal{J},k}}\frac{\partial e_{\mathcal{J},k}}{\partial\hat{W}_{\mathcal{J},k}} = \hat{W}_{\mathcal{J},k} - \alpha_\mathcal{J} e_{\mathcal{J},k}\tilde{\phi}_\mathcal{J}(\mathcal{X}_k), \tag{C9}$$

with $\alpha_u = diag\{0.2\}_{5\times5}$ and $\alpha_\mathcal{J} = diag\{0.05\}_{5\times5}$.

In this example, we examine the following two cases.

Case 1. In this case, we evaluate the prescribed performance by adjusting the parameters of the prescribed performance function.

Case 2. In this case, we adjust the relative weights between control effort and tracking error within the cost function to analyze the sensitivity of the control strategy to performance trade-offs.

The simulation results of Example 1 are presented in Figs. C1−C10 and Table C1. Figs. C1 and C6 indicate that the state always evolves within the prescribed boundary $-\rho_k < x_k < \rho_k$, thereby satisfying the desired transient and steady-state performance across all cases. As can be observed from Figs. C1, C3, and Table C1, different prescribed boundaries enable distinct performance specificationssuch as convergence time and steady-state valuesas well as varying cost function values. Furthermore, Figs. C6, C8, and Table C1 demonstrate that, in comparison with the prescribed boundaries, the weighting coefficients exert a more significant influence on the cost function. It is clearly evident from Figs. C2 and C7 that, in both scenarios, the computed control input u_k adheres to the predefined saturation constraint $|u_k| \leqslant \bar{u}$. Finally, Figs. C4, C5, C9, and C10 illustrate the convergence behavior of $\hat{W}_{u,k}$ and $\hat{W}_{\mathcal{J},k}$. In summary, the simulation results confirm that the proposed method achieves optimal stabilization of the dynamic system, while ensuring that the state exhibits the desired prescribed performance and that the controller satisfies the given constraints.

Table C1 Comparisons of control performance in Example 1.

Cases	Design parameters	Cost function	Convergence time	Steady-state value
Case 1	$\rho_0 = 1.2, \rho_\mathcal{K} = 0.2, \mathcal{K} = 0.05$	0.33	$\leqslant 0.05$ s	$(-0.02, 0.17)$
$\mathcal{Q}_\mathcal{X} = 8, \mathcal{R}_u = 1$	$\rho_0 = 5, \rho_\mathcal{K} = 2, \mathcal{K} = 0.1$	0.14	$\leqslant 0.07$ s	$(-0.02, 0.28)$
$\lvert u\rvert \leqslant \bar{u} = 0.3$	$\rho_0 = 15, \rho_\mathcal{K} = 8, \mathcal{K} = 0.2$	0.13	$\leqslant 0.09$ s	$(-0.02, 0.45)$
Case 2	$\mathcal{Q}_\mathcal{X} = 1, \mathcal{R}_u = 100$	0.73	$\leqslant 0.05$ s	$(-0.01, 0.06)$
$\rho_0 = 1.2, \rho_\mathcal{K} = 0.2$	$\mathcal{Q}_\mathcal{X} = 1, \mathcal{R}_u = 1$	0.23	$\leqslant 0.05$ s	$(-0.01, 0.05)$
$\mathcal{K} = 0.05, \lvert u\rvert \leqslant 0.5$	$\mathcal{Q}_\mathcal{X} = 100, \mathcal{R}_u = 1$	1.1	$\leqslant 0.05$ s	$(-0.01, 0.04)$

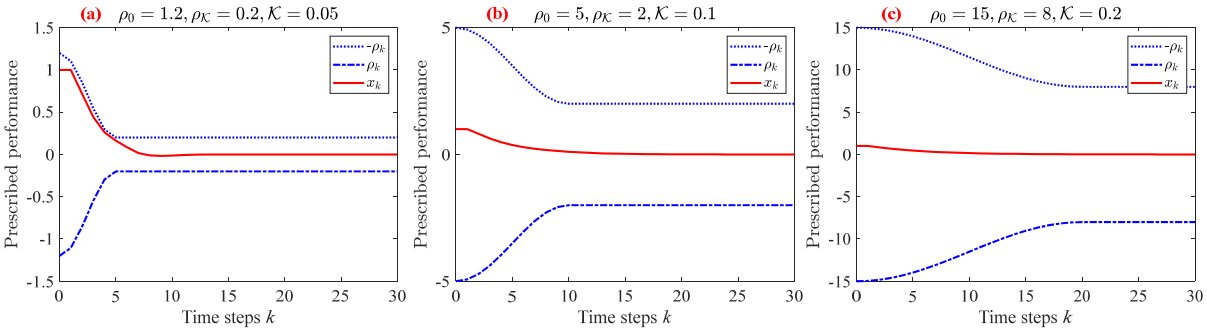

Figure C1 System state in Case 1.

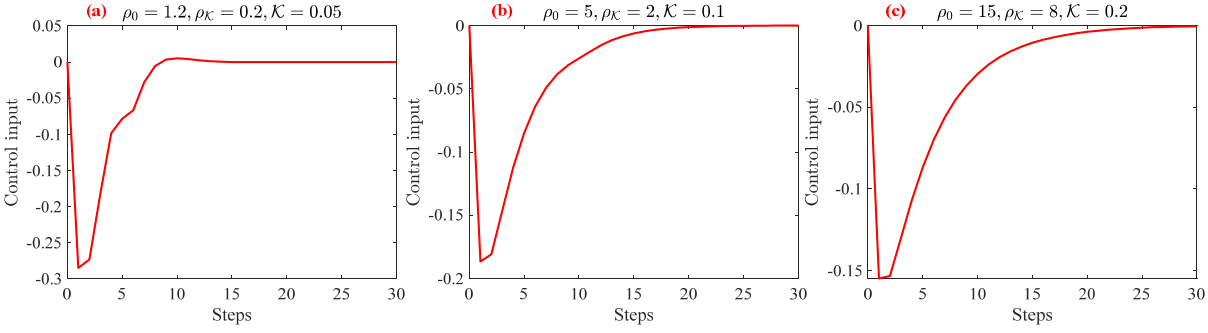

Figure C2 Control input in Case 1.

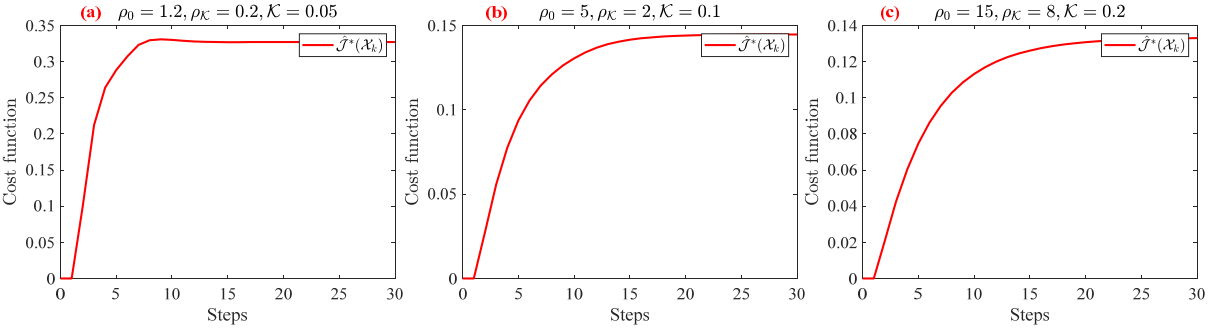

Figure C3 Cost function in Case 1.

Appendix C.2 Example 2

In this example, to further validate the superiority, the proposed controller is applied to the SSP (See Fig. C11.), and then is compared with a traditional proportional control (TPC) scheme and one existing PPC (EPPC) strategy which uses a traditional performance function [30]. The plant model of SSP is $x_{k+1} = f(x_k) + g(x_k)u_k$ with $x_k = [x_{1,k}, x_{2,k}]^\top \in \Re^2$, $f(x_k) = [x_{1,k} - 14.17T_s(x_{1,k} - x_{2,k}), x_{2,k} - 7.56T_s x_{1,k} - 82.26T_s x_{2,k}]^\top$, $g(x_k) = [0, 2.34T_s]^\top$, and $u_k \in \Re$. It is clear that $x_k = (0, 0)$ is the equilibrium state. We expect the state x_k to satisfy the prescribed performance $-\rho_{1,k} < x_{1,k} < \rho_{1,k}$ and

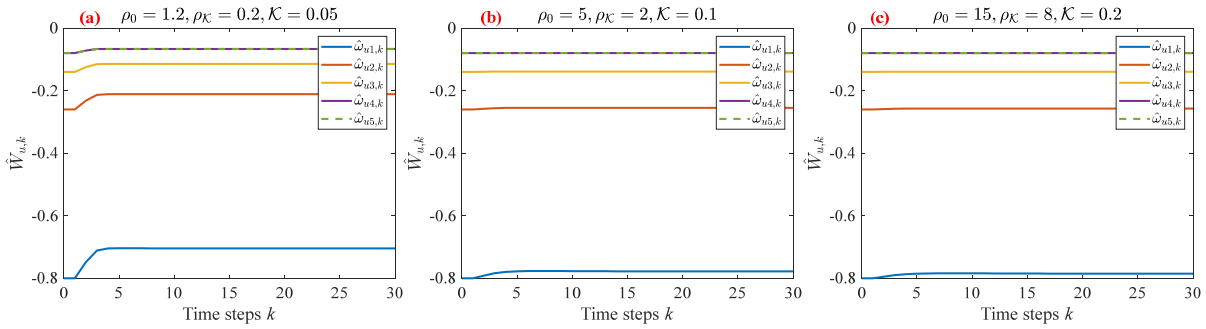

Figure C4 $\hat{W}_{u,k}$ in Case 1.

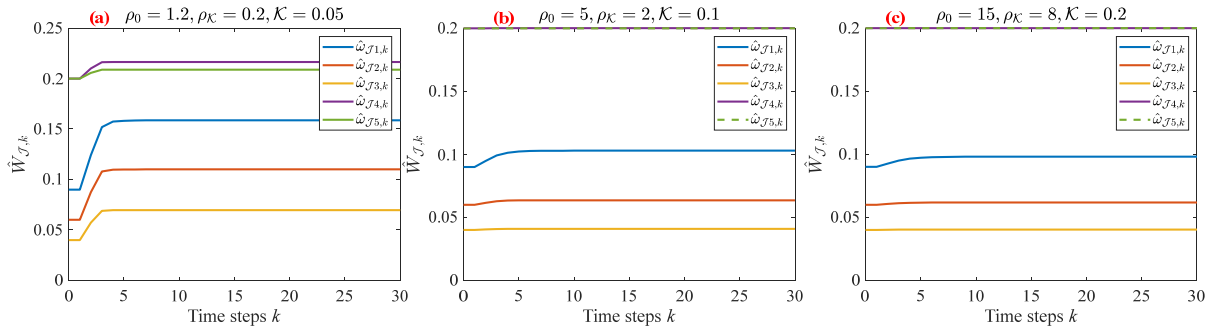

Figure C5 $\hat{W}_{\mathcal{J},k}$ in Case 1.

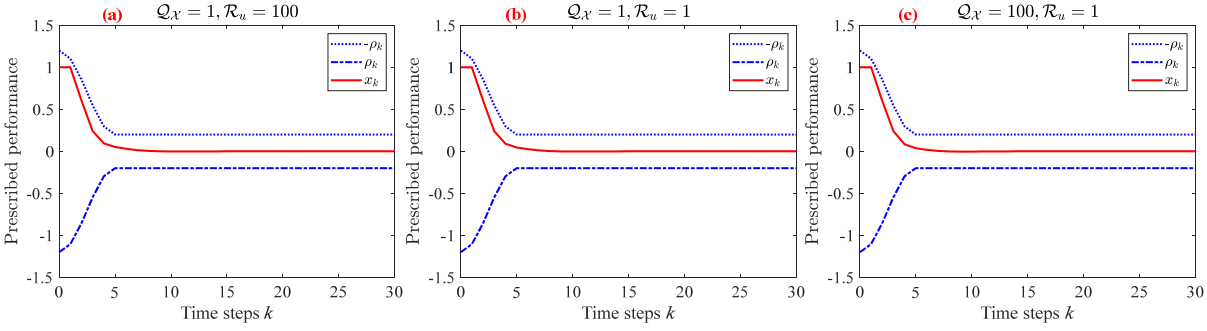

Figure C6 System state in Case 2.

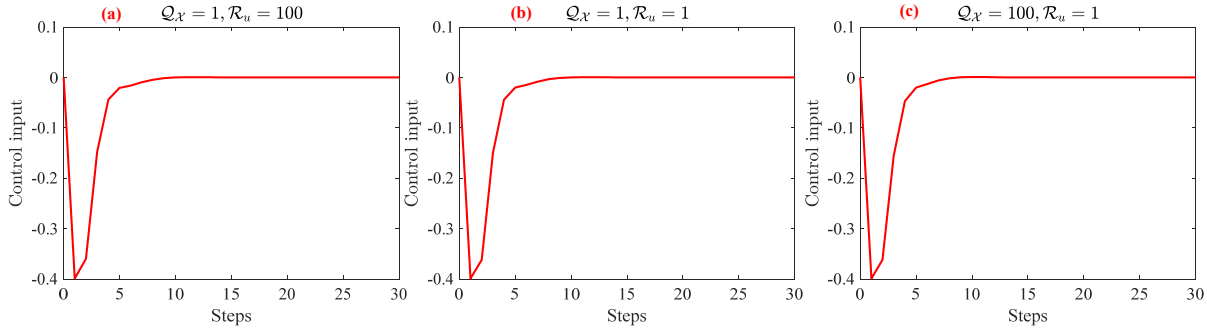

Figure C7 Control input in Case 2.

$-\rho_{2,k} < x_{2,k} < \rho_{2,k}$, with

$$\rho_{1,k} = \begin{cases} 0.5\tanh\left(\pi - \frac{2\pi}{12}k\right) + 0.7, k \leqslant 12 \\ 0.2, k > 12, \end{cases} \tag{C10}$$

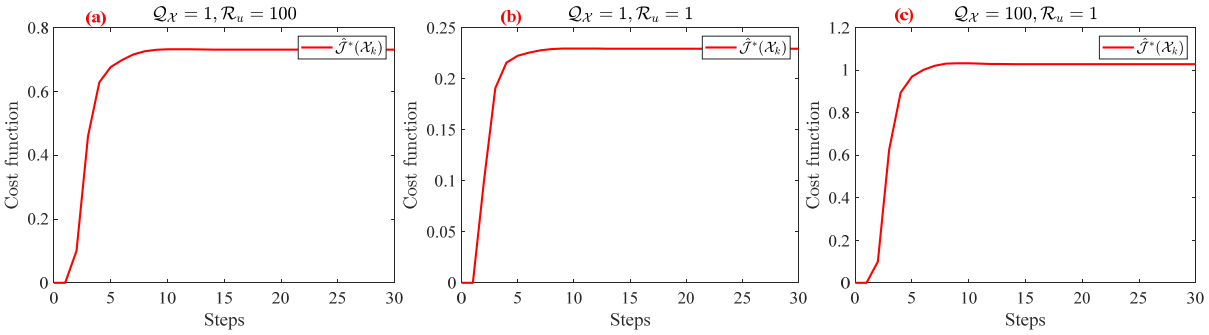

Figure C8 Cost function in Case 2.

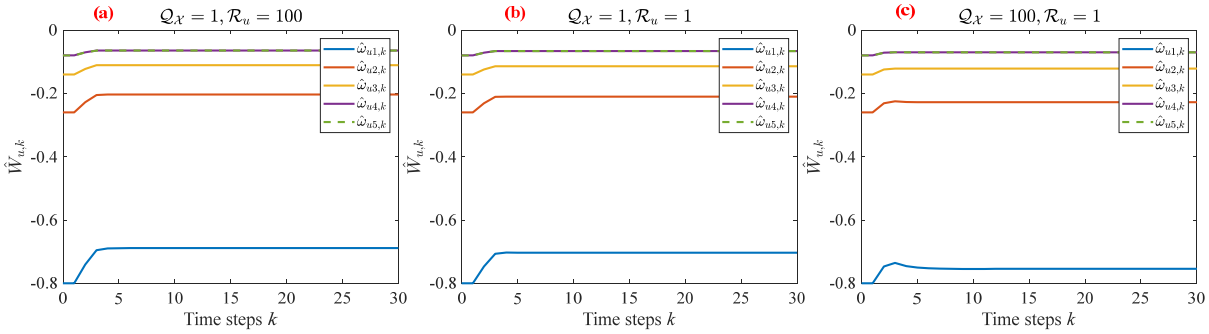

Figure C9 $\hat{W}_{u,k}$ in Case 2.

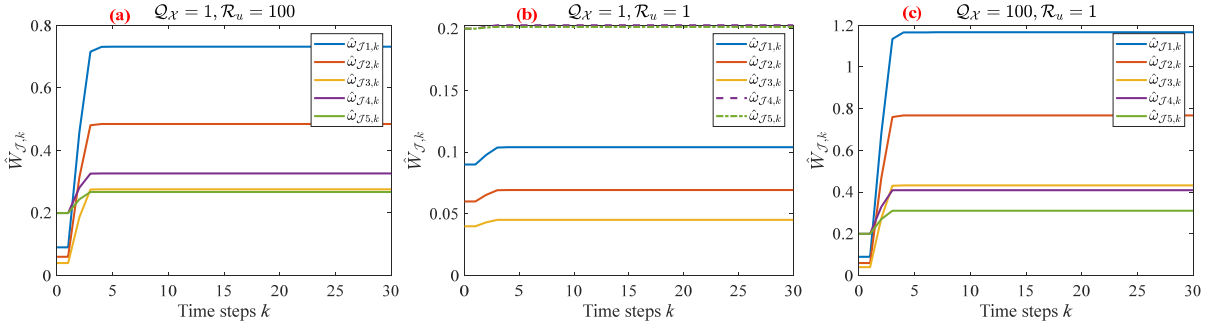

Figure C10 $\hat{W}_{\mathcal{J},k}$ in Case 2.

$$\rho_{2,k}=\begin{cases}0.5\tanh\left(\pi-\frac{2\pi}{2}k\right)+0.7, k\leqslant 2\\ 0.2, k>2.\end{cases} \tag{C11}$$

Define transformed errors $\alpha_{1,k}=\frac{1}{2}\ln\left(\frac{\rho_{1,k}+x_{1,k}}{\rho_{1,k}-x_{1,k}}\right)$ and $\alpha_{2,k}=\frac{1}{2}\ln\left(\frac{\rho_{2,k}+x_{2,k}}{\rho_{2,k}-x_{2,k}}\right)$. By the definition (B6), we derive new states $\mathcal{X}_{1,k+1}=\frac{e^{2\eta_1\alpha_{1,k}}-1}{1+e^{2\eta_1\alpha_{1,k}}}\rho_{1,k+1}$ and $\mathcal{X}_{2,k+1}=\frac{e^{2\eta_2\alpha_{2,k}}-1}{1+e^{2\eta_2\alpha_{2,k}}}\rho_{2,k+1}$, as well as the new dynamic system $\mathcal{X}_{k+1}=f(\mathcal{X}_k)+g(\mathcal{X}_k)u_k$ with $\mathcal{X}_k=[\mathcal{X}_{1,k},\mathcal{X}_{2,k}]^\top$, $f(\mathcal{X}_k)=[\mathcal{X}_{1,k}-14.17T_s(\mathcal{X}_{1,k}-\mathcal{X}_{2,k}),\mathcal{X}_{2,k}-7.56T_s\mathcal{X}_{1,k}-82.26T_s\mathcal{X}_{2,k}]^\top$, $g(\mathcal{X}_k)=[0,2.34T_s]^\top$, and $\eta_1=\eta_2=0.5$. All controllers use the same cost function $\mathcal{J}(\mathcal{X}_k)=\sum_{j=k}^{\infty}(\mathcal{X}_j^\top\mathcal{Q}_\mathcal{X}\mathcal{X}_j+\mathcal{W}(u_j))$ with $\mathcal{W}(u_j)=2\int_0^{u_j}\text{atanh}^\top\left(\frac{\tau}{\bar{u}}\right)\mathcal{R}_u\bar{u}d\tau=\mathcal{R}_u\bar{u}^2\ln\left(1-\frac{u_j^2}{\bar{u}^2}\right)+2\mathcal{R}_u\bar{u}u_j\text{atanh}\left(\frac{u_j}{\bar{u}}\right)$, $\mathcal{Q}_\mathcal{X}=[5,0.1;0.1,1]$, $\mathcal{R}_u=0.1$, and $\bar{u}=0.2$.

In this example, both the optimal controller u_k^* and the optimal cost function $\mathcal{J}^*(\mathcal{X}_k)$ are also approximately estimated as follows:

$$\hat{u}_k^*=\hat{W}_{u,k}^\top\phi_u(\mathcal{X}_k),\hat{\mathcal{J}}^*(\mathcal{X}_k)=\hat{W}_{\mathcal{J},k}^\top\phi_\mathcal{J}(\mathcal{X}_k), \tag{C12}$$

where $\hat{u}_k^*$ and $\hat{\mathcal{J}}^*(\mathcal{X}_k)$ represent the estimations of u_k^* and $\mathcal{J}^*(\mathcal{X}_k)$ with

$$\hat{W}_{u,k}=\left[\hat{\omega}_{u1,k},\hat{\omega}_{u2,k},\hat{\omega}_{u3,k},\hat{\omega}_{u4,k},\hat{\omega}_{u5,k},\ \hat{\omega}_{u6,k},\hat{\omega}_{u7,k},\hat{\omega}_{u8,k}\right]^\top\in\Re^8, \tag{C13}$$

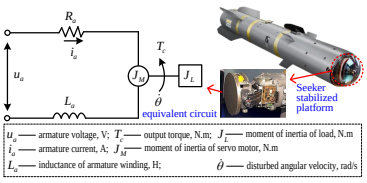

Figure C11 Seeker stabilized platform.

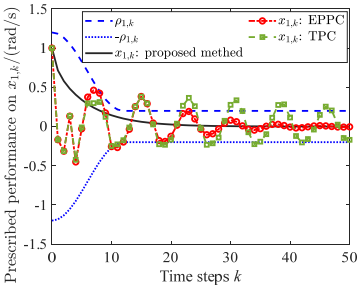

Figure C12 $x_{1,k}$ in Example 2.

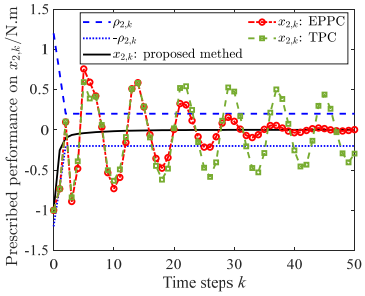

Figure C13 $x_{2,k}$ in Example 2.

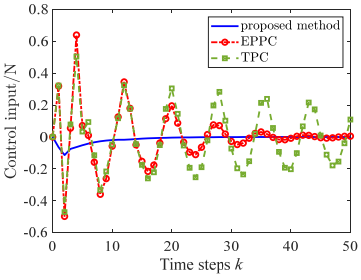

Figure C14 Control input in Example 2.

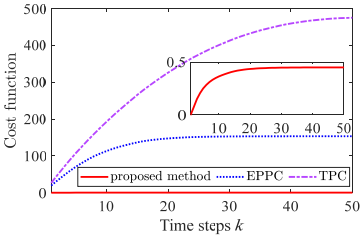

Figure C15 Cost function in Example 2.

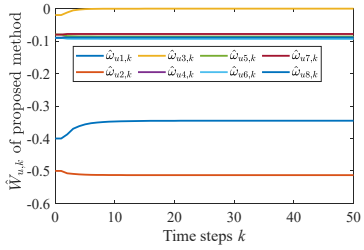

Figure C16 $\hat{W}_{u,k}$ in Example 2.

Table C2 Comparisons of control performance in Example 2.

Performance indicators		$x_{1,k}$	$x_{2,k}$
Overshoot	Proposed method	none	none
	EPPC	-0.45 rad/s	0.76 N.m
	TPC	-0.42 rad/s	0.59 N.m
Convergence time	Proposed method	$\leqslant 0.12$ s	$\leqslant 0.02$ s
	EPPC	$\geqslant 0.23$ s	$\geqslant 0.26$ s
	TPC	$\geqslant 0.5$ s	$\geqslant 0.5$ s
Steady-state value $t \in [0.2, 0.5]$ s	Proposed method	$(0, 0.03)$ rad/s	$(-3.5, 0) \times 10^{-3}$ N.m
	EPPC	$(0.15, 0.2)$ rad/s	$(-0.3, 0.4)$ N.m
	TPC	$(0.3, 0.4)$ rad/s	$(-0.6, 0.6)$ N.m
Cost function	Proposed method	0.45	
	EPPC	153.4	
	TPC	475.2	

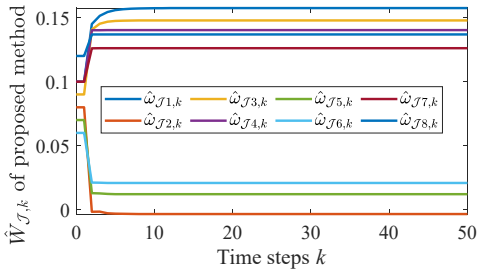

Figure C17 $\hat{W}_{\mathcal{J},k}$ in Example 2.

$$\hat{W}_{\mathcal{J},k} = \left[\hat{\omega}_{\mathcal{J}1,k}, \hat{\omega}_{\mathcal{J}2,k}, \hat{\omega}_{\mathcal{J}3,k}, \hat{\omega}_{\mathcal{J}4,k}, \hat{\omega}_{\mathcal{J}5,k},\ \hat{\omega}_{\mathcal{J}6,k}, \hat{\omega}_{\mathcal{J}7,k}, \hat{\omega}_{\mathcal{J}8,k}\right]^\top \in \Re^8, \tag{C14}$$

$$\phi_u(\mathcal{X}_k) = \phi_{\mathcal{J}}(\mathcal{X}_k) = \left[\mathcal{X}_{1,k}, \mathcal{X}_{2,k}, \mathcal{X}_{1,k}^2, \mathcal{X}_{2,k}^2, \mathcal{X}_{1,k}\mathcal{X}_{2,k},\ \mathcal{X}_{1,k}^2\mathcal{X}_{2,k}, \mathcal{X}_{1,k}\mathcal{X}_{2,k}^2, \mathcal{X}_{1,k}^2\mathcal{X}_{2,k}^2\right]^\top, \tag{C15}$$

$$\hat{W}_{u,0} = [-0.4, -0.5, -0.02, -0.09, -0.08,\ -0.09, -0.08, -0.09]^\top, \tag{C16}$$

$$\hat{W}_{\mathcal{J},0} = [0.1, 0.08, 0.09, 0.1, 0.07, 0.06, 0.1, 0.12]^\top. \tag{C17}$$

Define controller approximation error $e_{u,k}$ and cost function approximation error $e_{\mathcal{J},k}$ as

$$e_{u,k} = -\bar{u}\tanh\left(-\frac{1}{2\bar{u}}\mathcal{R}_u^{-1}g^\top(\mathcal{X}_k)\frac{\partial\hat{\mathcal{J}}^*(\mathcal{X}_{k+1})}{\partial\mathcal{X}_{k+1}}\right) + \hat{W}_{u,k}^\top\phi_u(\mathcal{X}_k), \tag{C18}$$

$$e_{\mathcal{J},k} = \mathcal{X}_k^\top\mathcal{Q}_{\mathcal{X}}\mathcal{X}_k + \mathcal{W}(u_k) + \hat{\mathcal{J}}^*(\mathcal{X}_{k+1}) - \hat{\mathcal{J}}^*(\mathcal{X}_k) = \mathcal{X}_k^\top\mathcal{Q}_{\mathcal{X}}\mathcal{X}_k + \mathcal{W}(u_k) + \hat{W}_{\mathcal{J},k}^\top\tilde{\phi}_{\mathcal{J}}(\mathcal{X}_k), \tag{C19}$$

with

$$\frac{\partial\hat{\mathcal{J}}^*(\mathcal{X}_{k+1})}{\partial\mathcal{X}_{k+1}} = \begin{bmatrix}\mathcal{B}_{21}\\ \mathcal{B}_{22}\end{bmatrix}, \tag{C20}$$

$$\begin{aligned}\mathcal{B}_{21} =& 2\hat{\omega}_{\mathcal{J}3,k}\mathcal{X}_{1,k+1} + \hat{\omega}_{\mathcal{J}5,k}\mathcal{X}_{2,k+1} + 2\hat{\omega}_{\mathcal{J}6,k}\mathcal{X}_{1,k+1}\mathcal{X}_{2,k+1}\\ &+ \hat{\omega}_{\mathcal{J}1,k} + \hat{\omega}_{\mathcal{J}7,k}\mathcal{X}_{2,k+1}^2 + 2\hat{\omega}_{\mathcal{J}8,k}\mathcal{X}_{1,k+1}\mathcal{X}_{2,k+1}^2,\end{aligned} \tag{C21}$$

$$\begin{aligned}\mathcal{B}_{22} =& 2\hat{\omega}_{\mathcal{J}4,k}\mathcal{X}_{2,k+1} + \hat{\omega}_{\mathcal{J}5,k}\mathcal{X}_{1,k+1} + 2\hat{\omega}_{\mathcal{J}7,k}\mathcal{X}_{1,k+1}\mathcal{X}_{2,k+1}\\ &+ \hat{\omega}_{\mathcal{J}6,k}\mathcal{X}_{1,k+1}^2 + 2\hat{\omega}_{\mathcal{J}8,k}\mathcal{X}_{1,k+1}^2\mathcal{X}_{2,k+1} + \hat{\omega}_{\mathcal{J}2,k},\end{aligned} \tag{C22}$$

$$\tilde{\phi}_{\mathcal{J}}(\mathcal{X}_k) = \phi_{\mathcal{J}}(\mathcal{X}_{k+1}) - \phi_{\mathcal{J}}(\mathcal{X}_k) = \begin{bmatrix}\mathcal{X}_{1,k+1} - \mathcal{X}_{1,k}\\ \mathcal{X}_{2,k+1} - \mathcal{X}_{2,k}\\ \mathcal{X}_{1,k+1}^2 - \mathcal{X}_{1,k}^2\\ \mathcal{X}_{2,k+1}^2 - \mathcal{X}_{2,k}^2\\ \mathcal{X}_{1,k+1}\mathcal{X}_{2,k+1} - \mathcal{X}_{1,k}\mathcal{X}_{2,k}\\ \mathcal{X}_{1,k+1}^2\mathcal{X}_{2,k+1} - \mathcal{X}_{1,k}^2\mathcal{X}_{2,k}\\ \mathcal{X}_{1,k+1}\mathcal{X}_{2,k+1}^2 - \mathcal{X}_{1,k}\mathcal{X}_{2,k}^2\\ \mathcal{X}_{1,k+1}^2\mathcal{X}_{2,k+1}^2 - \mathcal{X}_{1,k}^2\mathcal{X}_{2,k}^2\end{bmatrix}, \tag{C23}$$

$$\mathcal{X}_{1,k+1} = \mathcal{X}_{1,k} - 14.17T_s(\mathcal{X}_{1,k} - \mathcal{X}_{2,k}), \tag{C24}$$

$$\mathcal{X}_{2,k+1} = \mathcal{X}_{2,k} - 7.56T_s\mathcal{X}_{1,k} - 82.26T_s\mathcal{X}_{2,k} + 2.34T_s\hat{W}_{u,k}^\top\phi_u(\mathcal{X}_k). \tag{C25}$$

By the gradient-based adaptation [10], we aim to minimize $E_{u,k} = \frac{1}{2}e_{u,k}^2$ and $E_{\mathcal{J},k} = \frac{1}{2}e_{\mathcal{J},k}^2$ by defining the following adaptive laws for $\hat{W}_{u,k}$ and $\hat{W}_{\mathcal{J},k}$

$$\hat{W}_{u,k+1} = \hat{W}_{u,k} - \alpha_u \frac{\partial E_{u,k}}{\partial e_{u,k}} \frac{\partial e_{u,k}}{\partial \hat{W}_{u,k}} = \hat{W}_{u,k} - \alpha_u e_{u,k}\phi_u(\mathcal{X}_k), \tag{C26}$$

$$\hat{W}_{\mathcal{J},k+1} = \hat{W}_{\mathcal{J},k} - \alpha_{\mathcal{J}} \frac{\partial E_{\mathcal{J},k}}{\partial e_{\mathcal{J},k}} \frac{\partial e_{\mathcal{J},k}}{\partial \hat{W}_{\mathcal{J},k}} = \hat{W}_{\mathcal{J},k} - \alpha_{\mathcal{J}} e_{\mathcal{J},k}\tilde{\phi}_{\mathcal{J}}(\mathcal{X}_k), \tag{C27}$$

with $\alpha_u = diag\{0.35\}_{8\times 8}$ and $\alpha_{\mathcal{J}} = diag\{0.15\}_{8\times 8}$.

In this example, the effectiveness of the proposed method and its superiority over the existing TPC and EPPC methodologies are clearly demonstrated in Figs. C12−C17 and Table C2. As shown in Figs. C12, C13, and Table C2, the predefined performance specifications are successfully achieved by the proposed control strategy, which also exhibits improved transient and steady-state responses compared to the conventional TPC and EPPC methods. Fig. C14 illustrates that the control input generated by the proposed approach remains within the saturation constraint $|u_k| \leqslant \bar{u} = 0.2$, whereas the existing controllers violate this limit. Furthermore, the evolution of the cost function is provided in Fig. C15, and the system responses of $\hat{W}_{u,k}$ and $\hat{W}_{\mathcal{J},k}$ are depicted in Figs. C16 and C17.

Appendix D Conclusions

A prescribed-time performance optimal control strategy is investigated for discrete-time systems subject to actuator saturation, with application to hypersonic flight systems. Fixed-time performance functions are utilized to impose boundary constraints on system outputs, ensuring asymptotic regulation of transformed errors. This leads to the formulation of a new discrete-time dynamic system for optimal controller design. By introducing a novel cost function, saturated optimal control protocols are derived to guarantee the desired prescribed-time performance. The value iteration algorithm is employed to compute both the cost function and the control sequence for implementing the developed controller. Finally, the effectiveness of the proposed approach is validated through comparative simulations based on ADP. In our future work, the proposed method will be further applied to physical experiments to comprehensively validate its effectiveness.

Appendix E *

References

1 Bian J, Xia H, Yi J, Mu C, Si C. Finite-time neuro-optimal control for constrained nonlinear systems through reinforcement learning. Neurocomputing, 2025, 637: 130079
2 Zhang C, Zhang Q, He J. Distributed total-amount optimal coordinated control of multi-motors with input and output saturation. Journal of the Franklin Institute, 2023, 360: 9065-9083
3 Wang K, Lu F, Chen Z, Li J. Real-time optimal control for attitude-constrained solar sailcrafts via neural networks. Acta Astronautica, 2024, 216: 446-458
4 Chen L, Hao F. Optimal tracking control for unknown nonlinear systems with uncertain input saturation: A dynamic event-triggered ADP algorithm. Neurocomputing, 2024, 564: 126964
5 Huang Y, Zhang Z, Zhao S. Neural robust optimal tracking control for nonlinear state-constrained systems with input saturation and external disturbances. Applied Intelligence, 2025, 55: 792
6 Liu D, Wei Q, Yan P. Generalized policy iteration adaptive dynamic programming for discrete-time nonlinear systems. IEEE Transactions on Systems, Man, and Cybernetics: Systems, 2015, 45(12): 1577-1591
7 Wei Q, Liu D, Yang X. Infinite horizon self-learning optimal control of nonaffine discrete-time nonlinear systems. IEEE Transactions on Neural Networks and Learning Systems, 2015, 26(4): 866-879
8 Liu D, Wei Q. Policy Iteration adaptive dynamic programming algorithm for discrete-time nonlinear systems. IEEE Transactions on Neural Networks and Learning Systems, 2014, 25(3): 621-634
9 Al-Tamimi A, Lewis F L, Abu-Khalaf M. Discrete-time nonlinear HJB solution using approximate dynamic programming: convergence proof. IEEE Transactions on Systems, Man, and CyberneticsPart B: Cybernetics, 2008, 38(4): 943-949
10 Wei Q, Lewis F L, Liu D, Song R, Lin H. Discrete-time local value iteration adaptive dynamic programming: convergence analysis. IEEE Transactions on Systems, Man, and Cybernetics: Systems, 2018, 48(6): 875-891
11 Bu X, Qi Q. Fuzzy optimal tracking control of hypersonic flight vehicles via single-network adaptive critic design. IEEE Transactions on Fuzzy Systems, 2022, 30(1): 270-278
12 Wei Q, Zhu L, Li T, Liu D. A new approach to finite-horizon optimal control for discrete-time affine nonlinear systems via a pseudolinear method. IEEE Transactions on Automatic Control, 2022, 67(5): 2610-2617
13 Wang D, Wang J, Zhao M, Xin P, Qiao J. Adaptive multi-step evaluation design with stability guarantee for discrete-time optimal learning control. IEEE/CAA Journal of Automatica Sinica, 2023, 10(9): 1797-1809
14 Wei Q, Liu D, Lin Q, Song R. Adaptive dynamic programming for discrete-time zero-sum games. IEEE Transactions on Neural Networks and Learning Systems, 2018, 29(4): 957-969
15 Liu Y, Li S, Tong S, Chen C L P. Adaptive reinforcement learning control based on neural approximation for nonlinear discrete-time systems with unknown nonaffine dead-zone input. IEEE Transactions on Neural Networks and Learning Systems, 2019, 30(1): 295-305
16 Tang L, Liu Y, Chen C L P. Adaptive critic design for pure-feedback discrete-time MIMO systems preceded by unknown backlashlike hysteresis. IEEE Transactions on Neural Networks and Learning Systems, 2018, 29(11): 5681-5690
17 Wang M, Wang K, Huang L, Shi H. Observer-based event-triggered tracking control for discrete-time nonlinear systems using adaptive critic design. IEEE Transactions on Systems, Man, and Cybernetics: Systems, 2023, 53(9): 5393-5403
18 Luo B, Liu D, Wu H. Adaptive constrained optimal control design for data-based nonlinear discrete-time systems with critic-only structure. IEEE Transactions on Neural Networks and Learning Systems, 2018, 29(6): 2099-2111
19 Dong L, Zhong X, Sun C, He H. Adaptive event-triggered control based on heuristic dynamic programming for nonlinear discrete-time systems. IEEE Transactions on Neural Networks and Learning Systems, 2017, 28(7): 1594-1605
20 Bechlioulis C P, Rovithakis G A. Robust adaptive control of feedback linearizable MIMO nonlinear systems with prescribed performance. IEEE Transactions on Automatic Control, 2008, 53(9): 2090-2099
21 Bu X, Luo R, Cao Y, Lei H. Early Warnings and Envelope Adjustment-based Safety Flight Control With Application to Hypersonic Vehicles. IEEE Transactions on Intelligent Transportation Systems, 2025, 26(8): 12701-12711
22 Bu X, Luo R, Lv M, Lei H. Adaptive fuzzy safety control of hypersonic flight vehicles pursuing adaptable prescribed behaviors: a sensing and adjustment mechanism. IEEE Transactions on Fuzzy Systems, 2024, 32(12): 7050C7062
23 Yoshimura T. An approximate design of the prescribed performance control for uncertain discrete-time nonlinear strict-feedback systems. International Journal of Systems Science, 2020, 51(14): 2549-2562
24 Yoshimura T. Prescribed performance control for MIMO stochastic discrete-time nonlinear systems in a strict-feedback form using a set of noisy measurements. International Journal of Systems Science, 2022, 53(4): 689-703

25 Huang X, Dong Z, Zhang F, Zhang L. Discrete-time extended state observer-based model-free adaptive sliding mode control with prescribed performance. International Journal of Robust and Nonlinear Control, 2022, 32: 4816-4842
26 Dong H, Zhao X, Luo B. Optimal tracking control for uncertain nonlinear systems with prescribed performance via critic-only ADP. IEEE Transactions on Systems, Man, and Cybernetics: Systems, 2022, 52(1): 561-573
27 Zhao S, Wang J, Xu H, Wang B. ADP-based attitude-tracking control with prescribed performance for hypersonic vehicles. IEEE Transactions on Aerospace and Electronic Systems, 2023, 59(5): 6419-6431
28 Yang H, Hu Q, Dong H, Zhao X, Li D. Optimized data-driven prescribed performance attitude control for actuator saturated spacecraft. IEEE/ASME Transactions on Mechatronics, 2023, 28(3): 1616-1626
29 Ye J, Dong H, Bian Y, Qin H, Zhao X. ADP-based optimal control for discrete-time systems with safe constraints and disturbances. IEEE Transactions on Automation Science and Engineering, 2024, 22: 115-128
30 Treesatayapun C. Prescribed performance controller with affine equivalent model for a class of unknown nonlinear discrete-time systems. International Journal of Systems Science, 2021, 52(2): 334-349
31 Liu D, Yang G. Prescribed performance model-free adaptive integral sliding mode control for discrete-time nonlinear systems. IEEE Transactions on Neural Networks and Learning Systems, 2019, 30(7): 2222-2230
32 Nguyen M L, Chen X, Yang F. Discrete-time quasi-sliding mode control with prescribed performance function and its application to piezo-actuated positioning systems. IEEE Transactions on Industrial Electronics, 2018, 65(1): 942-950
33 Shao S, Chen M. Adaptive neural discrete-time fractional-order control for a UAV system with prescribed performance using disturbance observer. IEEE Transactions on Systems, Man, and Cybernetics: Systems, 2021, 51(2): 742-754
34 Treesatayapun C. Prescribed performance of discrete-time controller based on the dynamic equivalent data model. Applied Mathematical Modelling, 2020, 78: 366-382
35 Hou M, Wang Y, Han Y. Data-driven discrete terminal sliding mode decoupling control method with prescribed performance. Journal of the Franklin Institute, 2021, 358: 6612-6633
36 Bu X, Lei H. Fixed-time prescribed performance unknown direction control of discrete-time non-affine systems without Nussbaum-type function. IEEE Transactions on Automation Science and Engineering, 2024, 21(4): 7064-7072
37 Al-Tamimi A, Lewis F L. Discrete-time nonlinear HJB solution using approximate dynamic programming: convergence proof. Proceedings of the 2007 IEEE Symposium on Approximate Dynamic Programming and Reinforcement Learning, 2007: 38-43